MAPPING IONIZATION WITHIN AND ACROSS PROTOPLANETARY DISK ENVIRONMENTS

Deryl Long[1] and Advisor: Ilse Cleeves[1]

[1] *University of Virginia*
530 McCormick Rd.
Charlottesville, VA 22903, USA

Abstract

Planetary compositions are set by the gas, ice, and dust in the cold, dark midplanes of protoplanetary disks (PPDs) encircling young stars. Chemistry in these cold, planet-forming midplanes is primarily driven by ions, particularly those chemical pathways governing the formation of water and organics. Ion-driven chemistry is thus central to the evolution of the bulk carbon and oxygen reservoirs inherited by forming planets via solids and gas. Ionization also impacts the redistribution of planet-forming materials by driving transport through the disk via accretion and magneto-hydrodynamic (MHD) flows. Measuring ionization throughout a disk is crucial for understanding both possible planet compositions and planet-forming capabilities. Here we examine in detail the ionization environment of the DM Tau system– a T Tauri star with a large, structured protoplanetary disk. We use new and archival ALMA observations of HCO^+, $H^{13}CO^+$, and N_2H^+ to produce the first forward-modeled 2D ionization constraints for the DM Tau disk and provide key insights as to the main drivers of ionization in this system. We then extend our discussion towards unprecedented large surveys currently underway with ALMA and JWST which we expect to further illuminate the diversity of ionization across the PPD population.

Introduction

Ionization plays a critical role in the evolution of protoplanetary disks and the formation of planets within these environments. Ions drive the most rapid chemical reactions (Herbst & Klemperer 1973; Tielens & Hagen 1982) in the coldest regions of the disk where neutral-neutral reactions are less efficient. Sufficient ionization allows the gas to couple to magnetic field lines and in turn drives a disk wind (Blandford & Payne 1982) and/or the magneto-rotational instability (MRI; Balbus & Hawley 1991). Ionization is also a key input parameter for chemical models, the results of which are used to interpret observations of disks and in turn predict the compositions of forming planets (Eistrup et al. 2018; Price et al. 2020).

Ions are responsible for driving chemical complexity in the cold ($T < 50$ K) disk midplane, creating formation pathways for organics (Cleeves et al. 2016) and water (van Dishoeck et al. 2013). If disks cannot efficiently form water, nascent planets would have to rely solely on inherited water from the parent molecular cloud (Cleeves et al. 2014). Understanding the distribution of water ice in disks is important, as the habitability of Earth-like planets may depend on post-formation delivery of water ice from asteroids and comets.

Ionization is also an important parameter for constraining the physical processes that impact the evolution of planet-forming material within the disk. In well-ionized regions of the disk, turbulence is thought to be primarily driven by the MRI. In weakly-ionized regions of the disk, the strength and nature of turbulence will be modified by non-ideal effects, such as Ohmic diffusion (Fleming & Stone 2003; Gole et al. 2016), ambipolar diffusion (Simon et al. 2013b,a), and the Hall effect (Bai 2015; Simon et al. 2015). If ionization is low enough, then hydrodynamic instabilities such as the "vertical shear instability" (VSI; Nelson et al. 2013), "convective overstability" (COS; Klahr & Hubbard 2014), and the "zombie vortex instability" (ZVI; Marcus et al. 2015) affect the gas dynamics in a very different manner than do the magnetic effects (see e.g., Nelson et al. 2013; Melon Fuksman et al. 2023).

For planets to form, micron-sized dust grains must stick together to form aggregates and eventually planetesimals on size scales of ∼0.1–100 km. Several complications must be overcome in this process, including radial drift (Whipple 1972) and fragmentation (Blum 2018). The "streaming instability" is a promising mechanism for overcoming dust growth barriers, as dense collections of dust are able to form planetesimals via direct gravitational collapse (Youdin & Goodman 2005), although this mechanism can be suppressed by background turbulence (Chen & Lin 2020; Umurhan et al. 2020; Gole et al. 2020; Lim et al. 2023). The ionization state of the disk gas can influence the overall turbulence which can in turn effect planet formation.

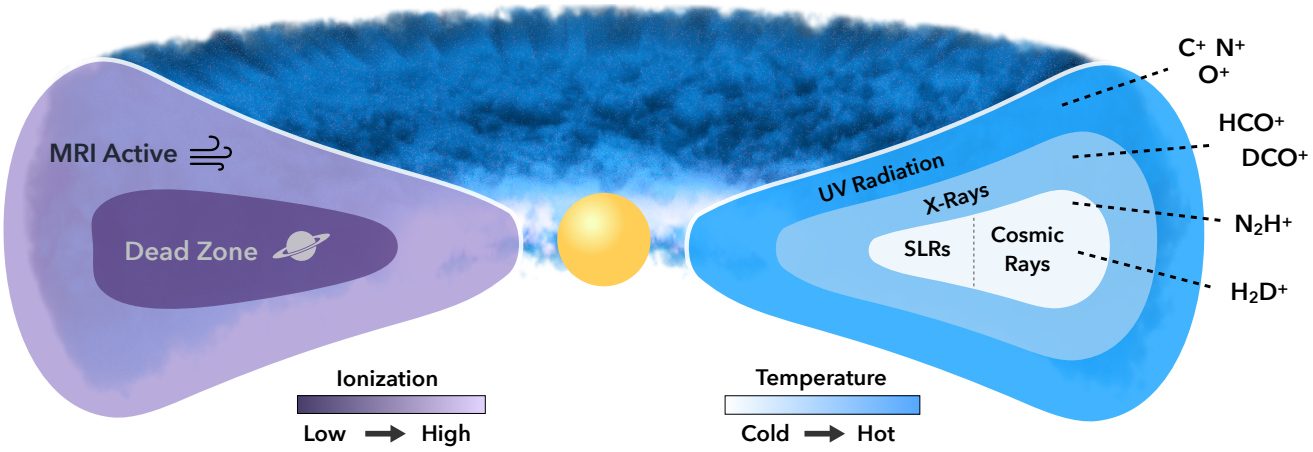

Figure 1. *Left: The degree of ionization sets the level of turbulence via MRI and determines presence of "dead zones"– regions in which the disk is not MRI active that are thought to be safe havens for planet formation (Gressel et al. 2012). Right: Dominant ionization processes and ionization tracing molecules in a typical protoplanetary disk. Modified from Miotello et al. (2022).*

Ionization in disks is driven by several sources including UV photons, X-rays, and cosmic rays (CRs). Each of these sources ionize different vertical and radial regions of the disk, and these regions are associated with different molecular ions (such as N_2H^+ and HCO^+) that are expected to be present at certain disk temperatures (Figure 1). UV photons drive ionization at the disk surface but are quickly attenuated at depths greater than 10^{-3} g cm^{-2} (Bergin et al. 2006). X-rays travel deeper into the disk, reaching depths from $\sim10^{-2}$ g cm^{-2} for soft X-rays (1 keV) to 1.6 g cm^{-2} for hard X-rays (10 keV). CRs can ionize column densities up to $\sim$100 g cm^{-2}, and are thus expected to be the most important sources of ionization in the most dense and cold regions of the disk where X-rays are strongly attenuated.

The rate of CR ionization in the dense ISM is on the order of 10^{-17} s^{-1} but this rate could be reduced by orders of magnitude due to CR exclusion by stellar winds or magnetic fields (Cleeves et al. 2013, 2015) or enhanced due to local particle acceleration (Padovani et al. 2015, 2016). Stars forming in clusters may be exposed to even stronger external radiation via CRs as well as external X-rays and UV photons (Clarke 2007; Adams 2010). Ultimately, navigating the complex picture of ionization across the 2D disk environment requires a merging of detailed dynamical and chemical models with reliable observational constraints.

Observations

Observations of different molecular tracers can be used to study ionization at different locations in the disk (see right hand side of Figure 1), though the reality is not so straightforward in observed sources due to the potential variations and complications discussed above. We used The Atacama Large Millimeter/sub-millimeter Array (ALMA) to observe molecular line and dust emission in DM Tau at radio frequencies. We present new observations of HCO^+ J=4–3, N_2H^+ J=4–3, and $H^{13}CO^+$ J=3–2. We also use archival data to constrain N_2H^+ J=3–2 (a detailed description of those observations and their calibration can be found in Qi et al. (2019)). The Band 7 HCO^+ 4–3 and N_2H^+ 4–3 data were taken on 2019 October 17-18 with 43 antennas covering 15m-740m baselines. These data were calibrated with the CASA Pipeline, with J0423-0120 as the band-pass calibrator and J0510+1800 as the phase calibrator. The Band 6 $H^{13}CO^+$ 3–2 data were taken on 2021 July 7 with 43 antennas covering 14m-2492m baselines.

We performed self-calibration, continuum subtraction, and imaging for all lines using CASA `v5.6.1`. For the line imaging of HCO^+we used Briggs weighting and a robust parameter of 0.5. For $H^{13}CO^+$ and N_2H^+ 4–3 we used natural weighting and a `uvtaper` of 0.″5 to maximize sensitivity. Following Qi et al. (2019) we imaged N_2H^+ 3–2 using natural weighting.

The data for N_2H^+ 4–3 was significantly more noisy than the other lines due to its close proximity to atmospheric water vapour features. We used the `matched_filter` command from the `VISIBLE`[1] Python package (Loomis et al. 2018) with our HCO^+ detection as a filter. We saw a 6σ response, indicating the presence of N_2H^+ 4–3. Though the N_2H^+4–3 line is not resolved in the observations we still include this line in our analysis. We create velocity integrated intensity (zeroth moment) maps (Figure 2) for the resolved detections using the `bettermoments`[2] Python package (Teague &

[1] https://github.com/AstroChem/VISIBLE
[2] https://github.com/richteague/bettermoments

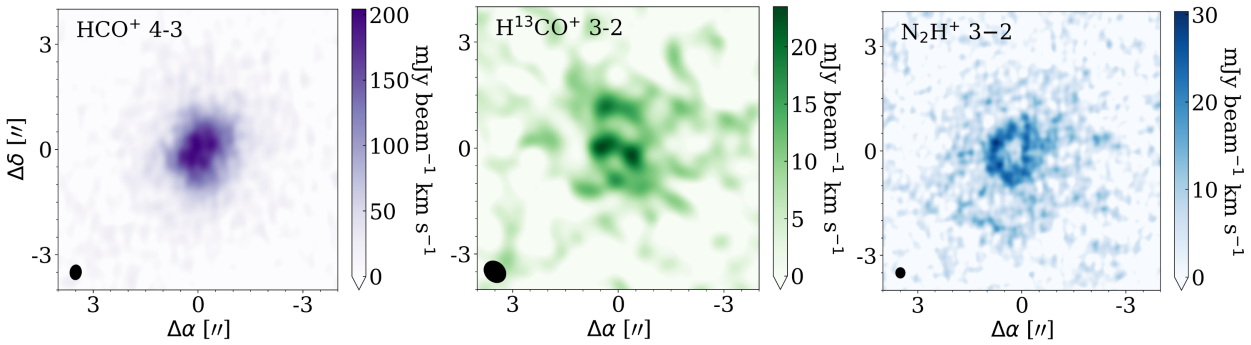

Figure 2. Integrated intensity (moment zero) maps for the resolved observations of HCO^+ 4–3, $H^{13}CO^+$ 3–2, and N_2H^+ 3–2. The beam is illustrated in the bottom left corner. Moment zero maps were produced using the `bettermoments` (Teague & Foreman-Mackey 2018) Python package.

Foreman-Mackey 2018). We produce radial line intensity profiles using the `GoFish`[3] Python package (Teague 2019) and discuss these in more detail in the "Results" section.

Modeling DM Tau

Our physical model combines a well-constrained gas density and temperature structure from Flaherty et al. (2020) with a dust structure based on continuum visibilities and spectral energy distribution (SED) fitting presented in Andrews et al. (2011). A detailed description of the gas density modeling and temperature parametrization can be found in Flaherty et al. (2020). The dust structure is derived from the azimuthally symmetric gas surface density profile

$$\Sigma_g = \Sigma_c \left(\frac{R}{R_c}\right)^{-\gamma} \exp\left[-\left(\frac{R}{R_c}\right)^{2-\gamma}\right], \quad (1)$$

where the characteristic scaling radius $R_c = 135$ au was determined by Andrews et al. (2011) and the surface density gradient is set to $\gamma = 1$. Our model assumes a global dust-to-gas ratio of $\xi = 0.01$. The dust disk has a flared vertical structure with a scale height distribution given by

$$H(r) = H_{100}\left(\frac{r}{100\text{ au}}\right)^{\psi} \quad (2)$$

where $H_{100} = 9.75$ au and $\psi = 1.2$. Following the SED fitting results in Andrews et al. (2011), we account for the disk's inner gap by depleting the dust by a factor $\delta_{cav} = 4.8$ in the region $R < R_{cav} = 19$ au. With the resulting surface density profile we calculate dust densities for small and large grains using the density distributions

$$\rho_s = \frac{(1-f)\Sigma_d}{\sqrt{2\pi}H} \exp\left[-\frac{1}{2}\left(\frac{z}{H}\right)^2\right] \quad (3)$$

and

$$\rho_l = \frac{f\Sigma_d}{\sqrt{2\pi}H\chi} \exp\left[-\frac{1}{2}\left(\frac{z}{\chi H}\right)^2\right], \quad (4)$$

where f and χ are settling parameters fixed at 0.85 and 0.2 respectively, meaning that large grains make up 85% of the total dust column and are distributed up to 20% of the disk scale height. Both the small and large dust grain populations follow an MRN size distribution (Mathis et al. 1977) within their respective size ranges.

Our models include ionization from three sources: UV photons, X-ray photons, and CRs. We exclude effects of inherited short-lived radionuclides (SLRs) for now since their initial abundance is uncertain and any inherited SLRs' rate of ionization will have decayed over DM Tau's estimated lifetime of ∼3–7 Myr (Simon et al. 2000), and ultimately should have negligible contributions to bulk disk ionization at the disk's current age.

Two-dimensional stellar X-ray and UV fluxes were obtained using the Bethell & Bergin (2011) Monte Carlo radiative transfer code and cross sections. We use an observed stellar UV spectrum for TW Hya and scale it to DM Tau's FUV luminosity by a factor of 2.16. We explore the effects of both quiescent and "flaring" X-ray states using template spectra from Cleeves et al. (2015). Both spectra are scaled to an X-ray luminosity of 2.5 $\times$ 10^{29} erg s^{-1} for DM Tau. Our X-ray models include energies from 1–20 keV. The quiescent and flaring states are distinguished by their respective hardness ratios, HR $= (L_{soft} - L_{hard})/(L_{soft} + L_{hard})$. The quiescent model (HR = -0.8) is soft X-ray dominated, while the hardened "flaring" model (HR = 0.3) is hard X-ray dominated.

We vary the rate of incident cosmic ray ionization by implementing five different CR–ionization rates (ζ_{CR}) listed in Table 1. Our two highest CR rates, M02 and W98, represent two different estimates of the local interstellar (LIS) cosmic ray spectrum. The Solar System Minimum-Modulation (SSM) and Maximum-

[3] https://github.com/richteague/gofish

Table 1. CR–ionization rates (ζ_{CR}) used for our modeling suite. Here "Min Mod" and "Max Mod" refer to the efficiency of modulation by stellar winds (Cleeves et al. 2013). In addition to the five ζ_{CR} values listed here, we also model two different X-ray conditions, yielding a modeling suite with a total of 10 models.

Cosmic Ray Model	Label	ζ_{CR}
Moskalenko et al. (2002)	M02	6.8×10^{-16}
Webber (1998)	W98	2.0×10^{-17}
Solar System Min Mod	SSM	1.1×10^{-18}
Solar System Max Mod	SSX	1.6×10^{-19}
T Tauri Max Mod	TTX	1.0×10^{-21}

Modulation (SSX) are based on measured CR rates on Earth, representing the CR ionization for our solar system given minimum and maximum amounts of CR modulation via stellar winds. Our lowest CR rate is the T Tauri Maximum-Modulation (TTX), which was extrapolated by Cleeves et al. (2013) to account for enhanced CR modulation by the higher stellar wind outflow rates measured for T Tauri stars. Additional details for the CR rates can be found in Cleeves et al. (2013).

Chemical abundances are calculated as a function of position and time using a 2D time–dependent rate equation chemical code from Fogel et al. (2011) adapted in Cleeves et al. (2014) and Anderson et al. (2021). The results presented in this work utilize our latest updated chemical network with 18,608 reactions and 1038 species, including deuterium isotopologues. Our initial abundances are representative of the chemical conditions in a typical molecular cloud. We run a grid of models using the physical structure and radiation fields described in Section 2. With five different CR ionization rates and two XR fields we have a total of ten models. Models are computed out to a time of 1 Myr, at which point the ion chemistry has settled into a pseudo-steady state. Figure 3 shows the resulting model column densities for N_2H^+ and HCO^+.

The resulting molecular abundances are input to the `LIME` non-LTE radiative transfer code (Brinch & Hogerheijde 2010) in order to calculate the emergent flux for HCO^+, N_2H^+, and $H^{13}CO^+$. We use collisional rates from the LAMDA database (Schöier et al. 2005; Daniel et al. 2005; Denis-Alpizar et al. 2020). The `LIME` code includes a doppler broadening parameter (b) that accounts for line broadening due to local turbulence. We set the doppler velocity as a function of the local sound speed (c_s), which is temperature dependent. For our "standard turbulence" models we use $b = 0.2c_s$. All of the

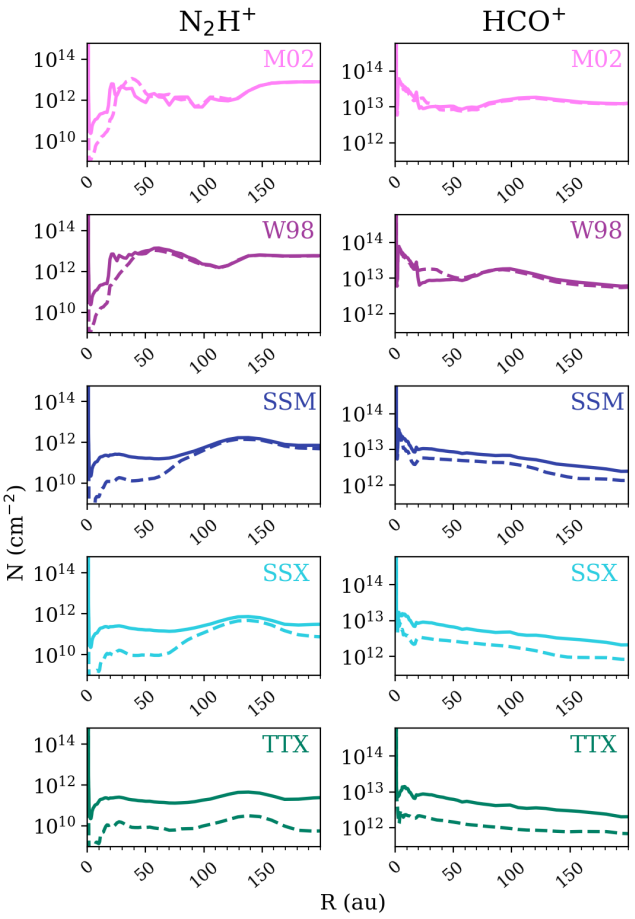

Figure 3. Vertically integrated radial column densities for N_2H^+ (left) and HCO^+ (right). The cosmic ray ionization rate decreases from top to bottom with labels corresponding to the rates listed in Table 1. Models with quiescent X-rays are shown with dashed lines while models with hardened X-rays are solid lines.

models assume a distance of 144.5 pc (Lindegren et al. 2018) and an inclination of 35.2° (Kudo et al. 2018).

We use `vis_sample` (Loomis et al. 2018) to perform visibility sampling of our LIME fits cubes. By using the ALMA measurement sets from our observations as inputs, we ensure that our simulated observations have the same uv coverage as the real observations. We perform continuum subtraction and image the model measurement sets in CASA `v.5.6.0` with the same parameters described in the "Observations" section. To make direct comparisons in the image plane, we produce radial profiles of the observed and modeled emission after imaging. Radial profiles are generated using the `radial_profile` function in the `GoFish` program (Teague 2019). We apply the same Keplerian masks used to image the observations and we integrate emission over the same velocity

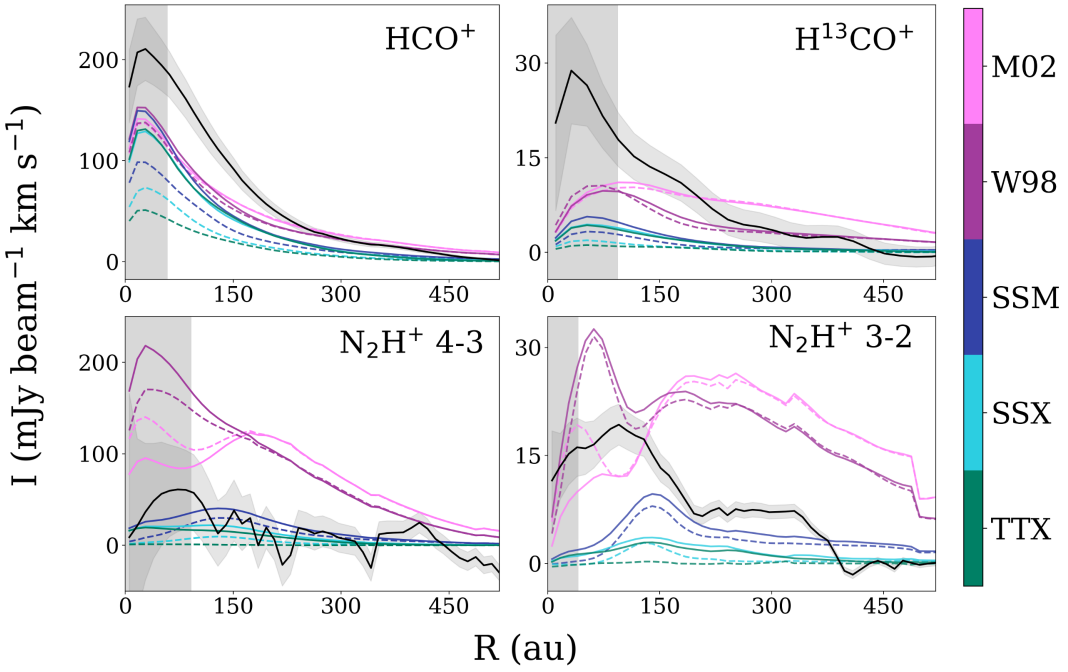

Figure 4. Observed and model radial profiles for the full disk. In each panel the solid black line is the observed emission profile and the associated light gray shading represents the uncertainties on the profile from `GoFish` plus the nominal 10% flux uncertainty from ALMA. The five different CR models are color coded according to the colorbar and labels on the right. For the models, dashed lines denote a quiescent XR spectrum while solid lines denote a hardened XR spectrum. The dark grey shading represents the beam of the data in au.

ranges used to produce the moment zero maps shown in Figure 2.

DM Tau Model Results

Observed emission reaches zero for all four lines by 500 au, so we consider radii < 500 au when calculating the global goodness of fit. Observed and model radial profiles for the full disk are shown in Figure 4. We find that the HCO^+ and $H^{13}CO^+$ tend to prefer a W98-F (high ionization rate) model, while in contrast, the N_2H^+ lines strongly prefer a SSM-F (reduced ionization rate) model. SSM-F is the best global fit ($\chi^2_{red,mean} = 13.8$) when we consider all four lines weighted equally. The observed emission profiles for all four lines are best fit by a model with a hard X-ray spectrum and a CR ionization rate of 1.1×10^{-18} s^{-1}.

Our modeling of HCO^+, $H^{13}CO^+$, and N_2H^+ suggests that a high rate of ionization by both CRs and X-rays is required to reproduce bright emission of molecular ions in the inner disk, while a low rate of ionization by CRs is required to fit the outer disk where the observed emission from all four lines is much more diffuse. This result is consistent with a strong ionized inner disk followed by a steep ionization gradient and a low ionization rate in the outer disk. Previous studies that suggest the presence of CR gradients in TW Hya and IM Lup (Cleeves et al. 2015; Seifert et al. 2021) found the opposite trend of ζ_{CR} suppression in the inner disk and, in the case of IM Lup, an increase in ζ_{CR} towards the outer disk. TW Hya is close to DM Tau in age (∼3–10 Myr; Vacca & Sandell 2011) and disk mass (0.05 $M_\odot$; Bergin et al. 2013) while IM Lup is both younger (1 Myr; Mawet et al. 2012) and more massive (∼0.1 $M_\odot$; Pinte et al. 2008). While both TW Hya and IM Lup exhibit substructure in their continuum emission (Huang et al. 2018), neither of these disks have a large inner cavity like DM Tau's 20 au gap.

The suppression of CR ionization in TW Hya and IM Lup can be explained by the presence of a disk wind blocking external ionizing radiation from reaching the inner disk. It is less straightforward to explain a CR gradient in the case of DM Tau, as we would not expect there to be a "barrier" blocking incident external CRs from reaching the outer disk while allowing them to ionize the inner disk. Rather than a reduced rate of ionization in the inner disk like IM Lup or TW Hya, DM Tau appears to have some kind of ionization enhancement localized to the inner ∼150 au.

Our global best fit model, SSM-F, is an intermediate ζ_{CR} model with a flaring X-ray state. This model comes closest to reproducing the bright emission from molecular ions in the inner disk without overproducing emission

from molecular ions in the outer disk. Our best-fit model suggests that the ionization fraction in DM Tau varies from $\chi_e > 1 \times 10^{-4}$ at the surface to $\chi_e < 1 \times 10^{-10}$ in the midplane, in agreement with previous estimates of DM Tau's ionization fraction (Öberg et al. 2011; Teague et al. 2015).

Our results do not suggest definitively that DM Tau's turbulence is MRI-driven or that the disk is uniquely turbulent due to an elevated degree of ionization compared to other systems. However, we do find that the inner disk is particularly well-ionized compared to the outer disk. The relatively high degree of ionization in the inner disk may be related to the large 20 au dust gap or another mechanism not captured by our modeling efforts. While we cannot identify the exact mechanism in this work, it is clear that ionizing radiation from the central star plays an important role in the inner disk and could play a role in driving DM Tau's previously discovered turbulence. Robust constraints on disk turbulence and ionization in larger samples will be critical for understanding the role of ionization in facilitating the redistribution of disk material via the MRI.

Surveying Ionization and Disk Chemistry

Characterizing ionization in individual sources is a powerful tool for understanding the chemistry and physics at play in protoplanetary disks. However, drawing statistical conclusions regarding the planet–forming capabilities and conditions in the "average" PPD requires a large sample of disks. Large surveys of disk chemistry are required to constrain the relationships between disk ionization and various properties such as disk size and morphology, and to in turn make connections to the observed population of exoplanets currently under study. We are taking major steps toward these broad goals with several large scale studies currently under way with ALMA and JWST.

The ALMA Cycle 9 Large Program the "Disk Exoplanet C/Onnection" (DECO; PI: Cleeves) recently observed a large sample of 80 disks around low mass (GKM-type; 0.2-1.5 $M_\odot$) stars – the most common exoplanet hosts – spanning the four best characterized SFRs within 200 pc: Lupus, ρ Ophiuchus, Chameleon I, and Taurus. DECO observations of molecular tracers, including N_2H^+, will constrain if and how disk chemistry varies across host star mass (M-dwarf vs. GK-dwarf), disk size, and SFR. Detections of N_2H^+ in a subset of the DECO disks in a single region, ChaI, are displayed in Figure 5. As data for all four regions is processed we will continue to build an unprecedented catalog of observations of this cold ionization tracer in the compact DECO disks. Given the diversity of ionization environments that we've seen in well-studied disks such as DM Tau, we expect that observations of such a large sample could reveal broad variations and/or trends in ionization across the disk population.

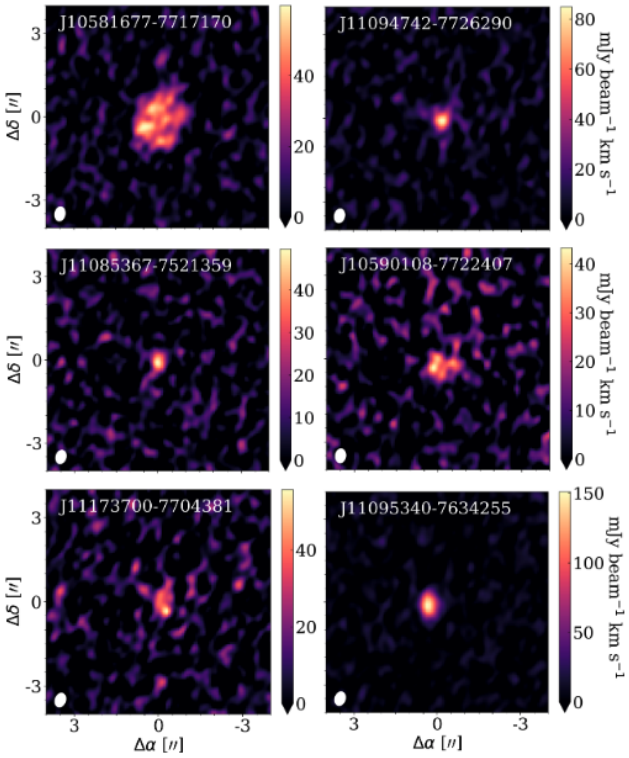

Figure 5. A subset of detections of N_2H^+ in six of the DECO ChaI disks.

In addition to observations from DECO, we are observing 40 of these same disks with an ALMA Cycle 10 program, the "Disk Ionization Survey to Constrain exoplanet Origins" (DISCO; PI: Long). With DISCO we aim to provide follow up observations of additional ionization tracers, namely HCO^+, for DECO sources in the Taurus and Lupus SFRs. In concert, the DECO and DISCO programs will provide observations of multiple ionization tracers, thus yielding comprehensive constraints on bulk disk ionization and allowing for the differentiation between ionization-driven chemistry at the surface (traced by HCO^+) vs. midplane (traced by N_2H^+) in a large sample. These ALMA observations will be further augmented by new and archival JWST MIRI observations of the 40 Taurus and Lupus disks. The JWST data will provide crucial insights as to the composition of the innermost regions of the disks- the terrestrial planet-forming zones. These observations, which are only possible with JWST at present, will allow our team to make concrete connections between disk chemistry (in both the inner and outer disk regions) and observed exoplanet compositions.

REFERENCES

Adams, F. C. 2010, ARA&A, 48, 47, doi: 10.1146/annurev-astro-081309-130830

Anderson, D. E., Blake, G. A., Cleeves, L. I., et al. 2021, ApJ, 909, 55, doi: 10.3847/1538-4357/abd9c1

Andrews, S. M., Wilner, D. J., Espaillat, C., et al. 2011, The Astrophysical Journal, 732, 42, doi: 10.1088/0004-637x/732/1/42

Bai, X.-N. 2015, The Astrophysical Journal, 798, 84

Balbus, S. A., & Hawley, J. F. 1991, ApJ, 376, 214, doi: 10.1086/170270

Bergin, E. A., Aikawa, Y., Blake, G. A., & van Dishoeck, E. F. 2006, The Chemical Evolution of Protoplanetary Disks. https://arxiv.org/abs/astro-ph/0603358

Bergin, E. A., Cleeves, L. I., Crockett, N. R., Favre, C., & Neill, J. L. 2013, in Astronomical Society of the Pacific Conference Series, Vol. 476, New Trends in Radio Astronomy in the ALMA Era: The 30th Anniversary of Nobeyama Radio Observatory, ed. R. Kawabe, N. Kuno, & S. Yamamoto, 185

Bethell, T. J., & Bergin, E. A. 2011, ApJ, 739, 78, doi: 10.1088/0004-637X/739/2/78

Blandford, R. D., & Payne, D. G. 1982, MNRAS, 199, 883, doi: 10.1093/mnras/199.4.883

Blum, J. 2018, SSRv, 214, 52, doi: 10.1007/s11214-018-0486-5

Brinch, C., & Hogerheijde, M. R. 2010, A&A, 523, A25, doi: 10.1051/0004-6361/201015333

Chen, K., & Lin, M.-K. 2020, The Astrophysical Journal, 891, 132, doi: 10.3847/1538-4357/ab76ca

Clarke, C. J. 2007, MNRAS, 376, 1350, doi: 10.1111/j.1365-2966.2007.11547.x

Cleeves, L. I., Adams, F. C., & Bergin, E. A. 2013, ApJ, 772, 5, doi: 10.1088/0004-637X/772/1/5

Cleeves, L. I., Bergin, E. A., Alexander, C. M. O., et al. 2014, Science, 345, 1590, doi: 10.1126/science.1258055

Cleeves, L. I., Bergin, E. A., Qi, C., Adams, F. C., & Öberg, K. I. 2015, ApJ, 799, 204, doi: 10.1088/0004-637X/799/2/204

Cleeves, L. I., Öberg, K. I., Wilner, D. J., et al. 2016, ApJ, 832, 110, doi: 10.3847/0004-637X/832/2/110

Daniel, F., Dubernet, M.-L., Meuwly, M., Cernicharo, J., & Pagani, L. 2005, Monthly Notices of the Royal Astronomical Society, 363, 1083, doi: 10.1111/j.1365-2966.2005.09542.x

Denis-Alpizar, O., Stoecklin, T., Dutrey, A., & Guilloteau, S. 2020, Monthly Notices of the Royal Astronomical Society, 497, 4276, doi: 10.1093/mnras/staa2308

Eistrup, C., Walsh, C., & van Dishoeck, E. F. 2018, AAP, 613, A14, doi: 10.1051/0004-6361/201731302

Flaherty, K., Hughes, A. M., Simon, J. B., et al. 2020, ApJ, 895, 109, doi: 10.3847/1538-4357/ab8cc5

Fleming, T., & Stone, J. M. 2003, The Astrophysical Journal, 585, 908, doi: 10.1086/345848

Fogel, J. K. J., Bethell, T. J., Bergin, E. A., Calvet, N., & Semenov, D. 2011, ApJ, 726, 29, doi: 10.1088/0004-637X/726/1/29

Gole, D., Simon, J. B., Lubow, S. H., & Armitage, P. J. 2016, ApJ, 826, 18, doi: 10.3847/0004-637X/826/1/18

Gole, D. A., Simon, J. B., Li, R., Youdin, A. N., & Armitage, P. J. 2020, ApJ, 904, 132, doi: 10.3847/1538-4357/abc334

Gressel, O., Nelson, R. P., & Turner, N. J. 2012, MNRAS, 422, 1140, doi: 10.1111/j.1365-2966.2012.20701.x

Herbst, E., & Klemperer, W. 1973, ApJ, 185, 505, doi: 10.1086/152436

Huang, J., Andrews, S. M., Dullemond, C. P., et al. 2018, The Astrophysical Journal, 869, L42, doi: 10.3847/2041-8213/aaf740

Klahr, H., & Hubbard, A. 2014, ApJ, 788, 21, doi: 10.1088/0004-637X/788/1/21

Kudo, T., Hashimoto, J., Muto, T., et al. 2018, The Astrophysical Journal, 868, L5, doi: 10.3847/2041-8213/aaeb1c

Lim, J., Simon, J. B., Li, R., et al. 2023, arXiv e-prints, arXiv:2312.12508, doi: 10.48550/arXiv.2312.12508

Lindegren, L., Hernández, J., Bombrun, A., et al. 2018, A&A, 616, A2, doi: 10.1051/0004-6361/201832727

Loomis, R. A., Öberg, K. I., Andrews, S. M., et al. 2018, The Astronomical Journal, 155, 182, doi: 10.3847/1538-3881/aab604

Marcus, P. S., Pei, S., Jiang, C.-H., et al. 2015, ApJ, 808, 87, doi: 10.1088/0004-637X/808/1/87

Mathis, J. S., Rumpl, W., & Nordsieck, K. H. 1977, ApJ, 217, 425, doi: 10.1086/155591

Mawet, D., Absil, O., Montagnier, G., et al. 2012, A&A, 544, A131, doi: 10.1051/0004-6361/201219662

Melon Fuksman, J. D., Flock, M., & Klahr, H. 2023, arXiv e-prints, arXiv:2312.06882, doi: 10.48550/arXiv.2312.06882

Miotello, A., Kamp, I., Birnstiel, T., Cleeves, L. I., & Kataoka, A. 2022, in PPVII. https://arxiv.org/abs/2203.09818

Moskalenko, I. V., Strong, A. W., Ormes, J. F., & Potgieter, M. S. 2002, ApJ, 565, 280, doi: 10.1086/324402

Nelson, R. P., Gressel, O., & Umurhan, O. M. 2013, MNRAS, 435, 2610, doi: 10.1093/mnras/stt1475

Padovani, M., Hennebelle, P., Marcowith, A., & Ferrière, K. 2015, AAP, 582, L13, doi: 10.1051/0004-6361/201526874

Padovani, M., Marcowith, A., Hennebelle, P., & Ferrière, K. 2016, AAP, 590, A8, doi: 10.1051/0004-6361/201628221
Pinte, C., Padgett, D. L., Ménard, F., et al. 2008, AA, 489, 633, doi: 10.1051/0004-6361:200810121
Price, E. M., Cleeves, L. I., & Öberg, K. I. 2020, ApJ, 890, 154, doi: 10.3847/1538-4357/ab5fd4
Qi, C., Öberg, K. I., Espaillat, C. C., et al. 2019, ApJ, 882, 160, doi: 10.3847/1538-4357/ab35d3
Schöier, F. L., van der Tak, F. F. S., van Dishoeck, E. F., & Black, J. H. 2005, A&A, 432, 369, doi: 10.1051/0004-6361:20041729
Seifert, R. A., Cleeves, L. I., Adams, F. C., & Li, Z.-Y. 2021, ApJ, 912, 136, doi: 10.3847/1538-4357/abf09a
Simon, J. B., Bai, X.-N., Armitage, P. J., Stone, J. M., & Beckwith, K. 2013a, ApJ, 775, 73, doi: 10.1088/0004-637X/775/1/73
Simon, J. B., Bai, X.-N., Stone, J. M., Armitage, P. J., & Beckwith, K. 2013b, ApJ, 764, 66, doi: 10.1088/0004-637X/764/1/66
Simon, J. B., Lesur, G., Kunz, M. W., & Armitage, P. J. 2015, MNRAS, 454, 1117, doi: 10.1093/mnras/stv2070
Simon, M., Dutrey, A., & Guilloteau, S. 2000, The Astrophysical Journal, 545, 1034, doi: 10.1086/317838
Teague, R. 2019, The Journal of Open Source Software, 4, 1632, doi: 10.21105/joss.01632
Teague, R., & Foreman-Mackey, D. 2018, Research Notes of the American Astronomical Society, 2, 173, doi: 10.3847/2515-5172/aae265
Teague, R., Semenov, D., Guilloteau, S., et al. 2015, Astronomy &amp Astrophysics, 574, A137, doi: 10.1051/0004-6361/201425268
Tielens, A. G. G. M., & Hagen, W. 1982, AAP, 114, 245
Umurhan, O. M., Estrada, P. R., & Cuzzi, J. N. 2020, The Astrophysical Journal, 895, 4, doi: 10.3847/1538-4357/ab899d
Vacca, W. D., & Sandell, G. 2011, ApJ, 732, 8, doi: 10.1088/0004-637X/732/1/8
van Dishoeck, E. F., Herbst, E., & Neufeld, D. A. 2013, Chemical Reviews, 113, 9043, doi: 10.1021/cr4003177
Webber, W. R. 1998, ApJ, 506, 329, doi: 10.1086/306222
Whipple, F. L. 1972, in From Plasma to Planet, ed. A. Elvius, 211
Youdin, A. N., & Goodman, J. 2005, ApJ, 620, 459, doi: 10.1086/426895
Öberg, K. I., Boogert, A. C. A., Pontoppidan, K. M., et al. 2011, ApJ, 740, 109, doi: 10.1088/0004-637x/740/2/109